

Model Estimation and Control of Compliant Contact Normal Force

Morteza Azad¹, Valerio Ortenzi², Hsiu-Chin Lin¹, Elmar Rueckert³ and Michael Mistry¹

Abstract—This paper proposes a method to realize desired contact normal forces between humanoids and their compliant environment. By using contact models, desired contact forces are converted to desired deformations of compliant surfaces. To achieve desired forces, deformations are controlled by controlling the contact point positions. Parameters of contact models are assumed to be known or estimated using the approach described in this paper. The proposed methods for estimating the contact parameters and controlling the contact normal force are implemented on a LWR KUKA IV arm. To verify both methods, experiments are performed with the KUKA arm while its end-effector is in contact with two different soft objects.

I. INTRODUCTION

Dealing with soft or compliant environment is still a challenging problem in robotics. This is more challenging for humanoid robots if they want to rely on compliant contacts for the balancing task. In most of the previous studies on whole-body motion control of humanoid robots, contacts with the environment are assumed to be rigid [13], [15]–[18], [20]. This assumption results in zero acceleration of the contact points as long as the contact force constraints (i.e. unilaterality of the normal force and the friction cone) are satisfied. On the other hand, compliant (soft) contact assumption [4], [10], [21] implies that contact surfaces deform and consequently contact forces are functions of surface deformations. These functions, which are called contact models, express the dynamics of contact surfaces.

To interact with a compliant surface, robots need (i) reliable estimations of the dynamics of the contact, and also (ii) a suitable strategy to deal with and exploit those dynamics. Focusing on the second one in our previous work [3], we presented a balance control strategy for a humanoid robot standing on a compliant surface. Our proposed controller was designed to control the movements of contact points based on the assumption that an exact model of the contact is available for the controller beforehand. Since we do not have access to the exact model of the contact surface in practice, providing a reliable and accurate estimation of the model is vital for the controller to succeed.

In order to provide an accurate contact model, reliable estimations of both forces and movements at the contact point (surface deformation) are required. Given these two, this paper focuses on estimating the contact model and also exploiting the estimated model in order to control the compliant contact force. For both estimation and control parts, the components of compliant contact forces which are

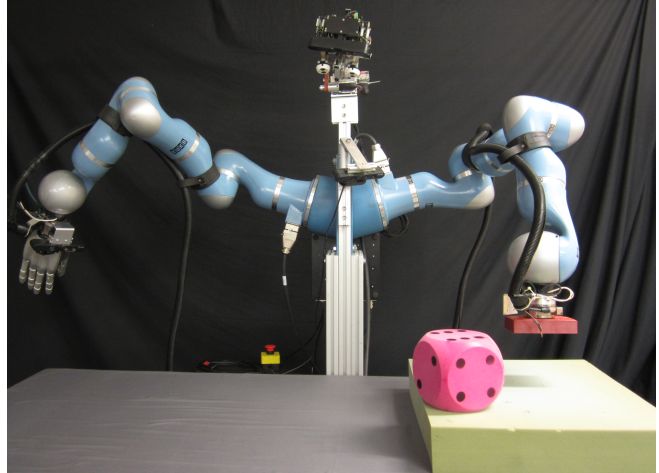


Fig. 1. KUKA LWR IV arms with two soft surfaces used in our experiments. The objects providing soft surfaces are sponge and dice.

normal to the contact surface are considered in this paper. We assume that, by controlling the normal components, we can always satisfy the friction cone constraints and therefore there will be no slipping at the contact surfaces.

A compliant contact model for the normal force is in fact a relationship between deformation at the contact surface in the direction of the normal vector, the rate of that deformation and the normal contact force. This relationship can be defined as a linear or a non-linear function. The linear model, which is known as Kelvin-Voigt in the literature [6], is defined as

$$f_z = \begin{cases} kz + \lambda\dot{z} & z \geq 0 \\ 0 & z < 0 \end{cases}, \quad (1)$$

where f_z is the normal contact force, z is the deformation at the contact point and k and λ are stiffness and damping coefficients, respectively. These two coefficients are the parameters of the contact model and are dependent on the mechanical properties of contact surfaces.

For the non-linear case, a few different models have been suggested in the literature which have the general form of

$$f_z = \begin{cases} kz^a + \lambda z^b \dot{z}^c & z \geq 0 \\ 0 & z < 0 \end{cases}, \quad (2)$$

where a , b and c are constant parameters. Note that setting $a = c = 1$ and $b = 0$ in (2) yields the linear model. Most of the non-linear models are reviewed in [7]. Among them the Hunt-Crossley model [11] is the most popular one in the robotics community due to its higher consistency with the physics of the contact [5], [8]. In this model, the constant parameters are set to $a = b = \frac{3}{2}$ and $c = 1$. Different learning

¹School of Computer Science and ²Mechanical Engineering, University of Birmingham, Edgbaston, Edgbaston, B15 2TT, The United Kingdom.

³Intelligent Autonomous Systems, TU Darmstadt, Darmstadt, Germany. contact email: m.azad at bham.ac.uk

methods have been suggested in the literature in order to estimate the parameters of this model [9], [19]. Recently, it is shown in [1] and [2] that setting $b = \frac{1}{2}$ in the model leads to more accurate results. This model is referred as Azad-Featherstone non-linear model in this paper.

The three above mentioned contact models: (i) Kelvin-Voigt, (ii) Hunt-Crossley and (iii) Azad-Featherstone, are used in our experiments to estimate the dynamics of two soft surfaces. These surfaces are provided by sponge and dice objects shown in Fig. 1. The best model for each surface, in terms of fitting the actual data, is selected to control the contact normal force between the robot's end-effector and the corresponding object. This is done by converting desired forces to desired deformations via contact models and realizing those deformations by the controller.

In Section II of this paper, we explain how controlling the normal component of the compliant contact force can be included in a whole-body motion control framework of a humanoid. Then, in section III, we show by experimental results how we can estimate compliant contact models between a LWR KUKA arm's end-effector and two different soft surfaces and control compliant contact forces in practice.

II. CONTROL STRATEGY

Consider a floating base robot which has multiple contacts with its environment. These contacts are combinations of rigid and compliant ones. Let $\mathbf{q} \in \mathbb{R}^n$ denote the vector of generalized coordinates of the robot which includes m actuated joints and 6 virtual degrees of freedom (DoF) due to the floating base ($n = m + 6$). Therefore, motion equations for this robot will be

$$\mathbf{M}\ddot{\mathbf{q}} + \mathbf{h} = \mathbf{B}\boldsymbol{\tau} + \mathbf{J}_s^T \mathbf{f}_s + \mathbf{J}_r^T \mathbf{f}_r, \quad (3)$$

where $\mathbf{M} \in \mathbb{R}^{n \times n}$ is the joint-space inertia matrix, $\mathbf{h} \in \mathbb{R}^n$ is the vector of Coriolis, centrifugal and gravity forces, $\mathbf{B} \in \mathbb{R}^{n \times m}$ is the selection matrix for actuated joints, $\boldsymbol{\tau} \in \mathbb{R}^m$ is the vector of joint torques, $\mathbf{J}_s \in \mathbb{R}^{6l_s \times n}$ and $\mathbf{J}_r \in \mathbb{R}^{6l_r \times n}$ are the Jacobians, and $\mathbf{f}_s \in \mathbb{R}^{6l_s}$ and $\mathbf{f}_r \in \mathbb{R}^{6l_r}$ are contact force vectors of the soft and rigid surfaces, respectively. Note that, at each contact point, the contact force is a 6×1 vector, and l_s and l_r are the numbers of points in contact with soft and rigid surfaces, respectively.

Since \mathbf{f}_s depends on the dynamics of the compliant surfaces, it is a known variable in the current time instant and is assumed to be measured or reliably estimated via force/torque sensors. Given that

$$\mathbf{J}_r \dot{\mathbf{q}} = \mathbf{0} \implies \dot{\mathbf{J}}_r \dot{\mathbf{q}} + \mathbf{J}_r \ddot{\mathbf{q}} = \mathbf{0}, \quad (4)$$

due to the rigid contacts, both unknown variables $\ddot{\mathbf{q}}$ and \mathbf{f}_r can be written separately as functions of $\boldsymbol{\tau}$ via (3). Finding proper values for $\boldsymbol{\tau}$ (usually via optimization techniques subject to the contact force constraints) to realize the desired values of $\ddot{\mathbf{q}}$ and \mathbf{f}_r , is the problem of whole-body motion control that is well-studied in the literature [16]. The desired values of $\ddot{\mathbf{q}}$ and \mathbf{f}_r are defined in order to maintain balance and execute manipulation tasks.

Controlling compliant contact forces for humanoid robots can be accomplished by adding a new task into the whole-body motion control framework. As we previously proposed in [3], this task could be controlling the movements of the contact points. Hence, a relationship between contact points accelerations and the control input ($\boldsymbol{\tau}$) is required. For soft contacts we have

$$\mathbf{J}_s \dot{\mathbf{q}} = \dot{\mathbf{p}} \implies \dot{\mathbf{J}}_s \dot{\mathbf{q}} + \mathbf{J}_s \ddot{\mathbf{q}} = \ddot{\mathbf{p}}, \quad (5)$$

where $\mathbf{p} \in \mathbb{R}^{6l_s}$ is the position vector of the compliant contact points expressed in the inertial frame. Note that \mathbf{p} includes both linear (denoted by $\mathbf{r} \in \mathbb{R}^{3l_s}$ in this paper) and angular parts of the position vector. By replacing $\ddot{\mathbf{q}}$ from (5) into (3) and solving for $\ddot{\mathbf{p}}$, we will have

$$\ddot{\mathbf{p}} = \boldsymbol{\alpha}_p \boldsymbol{\tau} + \boldsymbol{\beta}_p, \quad (6)$$

where

$$\begin{aligned} \boldsymbol{\alpha}_p &= \mathbf{J}_s \mathbf{M}^{-1} \mathbf{B} - \mathbf{J}_s \mathbf{M}^{-1} \mathbf{J}_r^T (\mathbf{J}_r \mathbf{M}^{-1} \mathbf{J}_r^T)^{-1} (\mathbf{J}_r \mathbf{M}^{-1} \mathbf{B}) \\ \boldsymbol{\beta}_p &= \mathbf{J}_s \mathbf{M}^{-1} \mathbf{J}_s^T \mathbf{f}_s - \mathbf{J}_s \mathbf{M}^{-1} \mathbf{h} + \dot{\mathbf{J}}_s \dot{\mathbf{q}} \\ &\quad - \mathbf{J}_s \mathbf{M}^{-1} \mathbf{J}_r^T (\mathbf{J}_r \mathbf{M}^{-1} \mathbf{J}_r^T)^{-1} (\mathbf{J}_r \mathbf{M}^{-1} \mathbf{J}_s^T \mathbf{f}_s \\ &\quad - \mathbf{J}_r \mathbf{M}^{-1} \mathbf{h} + \dot{\mathbf{J}}_r \dot{\mathbf{q}}) \end{aligned}$$

Thus, by using (6), we can define a task in order to control the motion of the contact points. This task can be achieved together with balance and manipulation tasks in a whole-body motion control framework.

As mentioned earlier, we are focusing on controlling the components of compliant contact forces which are normal to the contact surfaces. The other components are the friction forces (2×1 vectors) and the moments (3×1 vectors). The friction forces are assumed to be maintained inside the friction cone by controlling the normal component. Controlling the moments of a contact can be expressed as controlling the location of its center of pressure (CoP) which could be a possible extension of the current work.

To control the normal compliant contact force, we control linear accelerations of the contact points. Therefore,

$$\ddot{\mathbf{r}} = \boldsymbol{\alpha}_l \boldsymbol{\tau} + \boldsymbol{\beta}_l, \quad (7)$$

where $\boldsymbol{\alpha}_l$ and $\boldsymbol{\beta}_l$ are obtained by selecting the relevant (to linear position) rows of $\boldsymbol{\alpha}_p$ and $\boldsymbol{\beta}_p$, respectively. This can also be done by replacing \mathbf{J}_s by \mathbf{J}_{s_l} in $\boldsymbol{\alpha}_p$ and $\boldsymbol{\beta}_p$, where \mathbf{J}_{s_l} is the matrix of the selected rows (corresponding to linear positions) of \mathbf{J}_s , implying that, $\dot{\mathbf{r}} = \mathbf{J}_{s_l} \dot{\mathbf{q}}$.

Given the normal vectors of the compliant contact surfaces which are denoted by \mathbf{n}_i (where $i = 1, 2, \dots, l_s$), we can calculate the normal force component and also the position and velocity in the normal direction of each surface. Let \mathbf{u}_i and \mathbf{r}_i denote the linear parts of the force and position vectors of the i^{th} compliant contact, respectively. They can be obtained directly from \mathbf{r} and \mathbf{f}_s . Hence,

$$f_i = \mathbf{u}_i^T \mathbf{n}_i, \quad (8)$$

where f_i is the contact normal force at the i^{th} compliant contact. Position and velocity of the i^{th} contact point in

its normal direction are $r_{z_i} = \mathbf{r}_i^T \mathbf{n}_i$ and $\dot{r}_{z_i} = \dot{\mathbf{r}}_i^T \mathbf{n}_i$, respectively. Note that the surface deformation and the rate of the deformation can be computed via

$$z_i = r_{z_i} - \mathbf{d}_i^T \mathbf{n}_i = (\mathbf{r}_i - \mathbf{d}_i)^T \mathbf{n}_i, \quad (9)$$

and

$$\dot{z}_i = \dot{r}_{z_i} = \dot{\mathbf{r}}_i^T \mathbf{n}_i, \quad (10)$$

for the i^{th} contact point, where \mathbf{d}_i is the position of the contact point at the beginning of the contact. This position is assumed to be known either from the geometry of the contact surface or the estimation of the starting instant of the contact by using force/torque or tactile sensors.

By using a contact model, we convert the desired normal compliant force to the desired deformation of the contact surface in the normal direction as $f_i^{cmd} = F(z_i^{cmd}, \dot{z}_i^{cmd})$, where F could be either (1) or (2). Then, we use a feedback controller to control the desired acceleration of the surface deformation (and consequently the contact point position) as

$$\ddot{z}_i^{des} = \ddot{z}_i^{cmd} + k_z(z_i^{cmd} - z_i) + k_{\dot{z}}(\dot{z}_i^{cmd} - \dot{z}_i), \quad (11)$$

where k_z and $k_{\dot{z}}$ are the controller gains. Note that not all arbitrary force profiles are physically achievable, since the contact forces follow the dynamics of the contact surfaces estimated by a first-order differential equation. We can extract $\ddot{\mathbf{r}}^{des}$ from \ddot{z}^{des} by differentiating (10) and then multiplying both sides by \mathbf{n}_i (i. e. $\ddot{z}_i \mathbf{n}_i = \ddot{\mathbf{r}}_i^T$). Given that $\mathbf{r} = [\mathbf{r}_1^T \ \mathbf{r}_2^T \ \dots \ \mathbf{r}_{l_s}^T]^T$, we have

$$\ddot{\mathbf{r}}^{des} = [\ddot{z}_1^{des} \mathbf{n}_1, \ddot{z}_2^{des} \mathbf{n}_2, \dots, \ddot{z}_{l_s}^{des} \mathbf{n}_{l_s}]^T. \quad (12)$$

By plugging (12) into (7), we can compute the desired joint torques which realize the desired accelerations of the contact points and therefore the desired contact forces at the compliant contacts.

III. EXPERIMENTS

In order to verify our strategy for controlling compliant contact forces in practice, we carry out a series of experiments with our KUKA LWR IV arm in contact with two different soft surfaces, including a sponge and a dice. These two objects are shown in Fig. 1 together with the robot. For each surface, we performed two types of experiments, which are referred as (i) *identification* and (ii) *control* experiments. The purpose of the identification, which is presented in subsection III-B, was to choose a proper model (either linear or non-linear) for each contact surface and estimate the model parameters. In the control experiments in subsection III-C, we aimed at controlling the normal compliant contact force given the estimated model from the identification experiments.

To provide reliable estimation of the contact forces, a 6-axis force-torque (F/T) sensor (Gamma, ATI, USA) is mounted on the end-effector of our KUKA LWR IV arm. A 3D plastic printed box (i.e. the robot's hand) is attached to the F/T sensor. The hand provides a flat surface to make contact with the soft objects. In the beginning of each experiment, the hand is placed about 4cm above the objects with its sole parallel to the horizontal plane.

A. KUKA Arm's Motion Control with A Compliant Contact

Since there is no under-actuation or rigid contact, modifying the motion equations in (3) for our 7 DoF KUKA arm yields

$$\mathbf{M}\ddot{\mathbf{q}} + \mathbf{h} = \boldsymbol{\tau} + \mathbf{J}_s^T \mathbf{f}_s. \quad (13)$$

In this experiment, the only contact is the one at the end-effector. Thus, (6) becomes

$$\ddot{\mathbf{p}} = (\mathbf{J}_s \mathbf{M}^{-1}) \boldsymbol{\tau} + \dot{\mathbf{J}}_s \dot{\mathbf{q}} - \mathbf{J}_s \mathbf{M}^{-1} \mathbf{h} + \mathbf{J}_s \mathbf{M}^{-1} \mathbf{J}_s^T \mathbf{f}_s. \quad (14)$$

As explained in Section II, to control the normal component of the contact force, we control the linear accelerations of the end-effector. The desired linear accelerations ($\ddot{\mathbf{r}}^{des}$) are computed from (12). In order to keep the CoP as close as possible to the center of the hand and provide a uniform contact, we start our experiments with the hand parallel to the surface and keep its orientation during the experiment. This is done by setting the desired angular positions to the initial ones. Therefore, by inverting (14), we define the control input as

$$\boldsymbol{\tau} = (\mathbf{J}_s \mathbf{M}^{-1})^\# (\ddot{\mathbf{p}}^{des} - \dot{\mathbf{J}}_s \dot{\mathbf{q}} + \mathbf{J}_s \mathbf{M}^{-1} \mathbf{h} - \mathbf{J}_s \mathbf{M}^{-1} \mathbf{J}_s^T \mathbf{f}_s) + \mathbf{N} \boldsymbol{\tau}_0, \quad (15)$$

where $\#$ denotes the generalized pseudo-inverse, $\mathbf{N} = \mathbf{I} - (\mathbf{J}_s \mathbf{M}^{-1})^\# (\mathbf{J}_s \mathbf{M}^{-1})$ is the null space projection matrix and $\boldsymbol{\tau}_0$ is the joint-space impedance control torque which tries to keep the initial configuration. Vector $\ddot{\mathbf{p}}^{des}$ is a 6×1 vector which includes the desired linear positions ($\ddot{\mathbf{r}}^{des}$) and the desired angular ones.

B. Identification Experiments

In Section I, we discussed linear and non-linear compliant contact normal force models; however, it is not clear which model is optimal for the surfaces used in our experiments. In the identification experiments, we estimate the contact parameters of the surface with three different models including (i) Kelvin-Voigt, (ii) Hunt-Crossley, and (iii) Azad-Featherstone models, and evaluate how well these models fit the actual data. As mentioned earlier, the reason of choosing two non-linear models is that the popular Hunt-Crossley model is recently shown to be outperformed by the Azad-Featherstone model in fitting the empirical data of the contact between spheres and plates with different materials [2].

In the identification experiments, we command the robot's hand to push each soft surface with a predefined reference trajectory in the vertical direction. Examples of reference trajectories along with the actual movements of the end-effector in the vertical direction for both sponge and dice are shown in Fig. 2. Each trajectory consists of two ramps at the beginning and the end, to make and break contacts, and a sine function with the frequency of 2π Hz in the middle. Red lines in the plots show the contact surfaces just before making the contact, which is estimated by using measured normal contact force (at the instant that the normal force goes above 1N). The maximum deformation for the dice is set to 7cm, whereas it is set to 5cm for the sponge to avoid

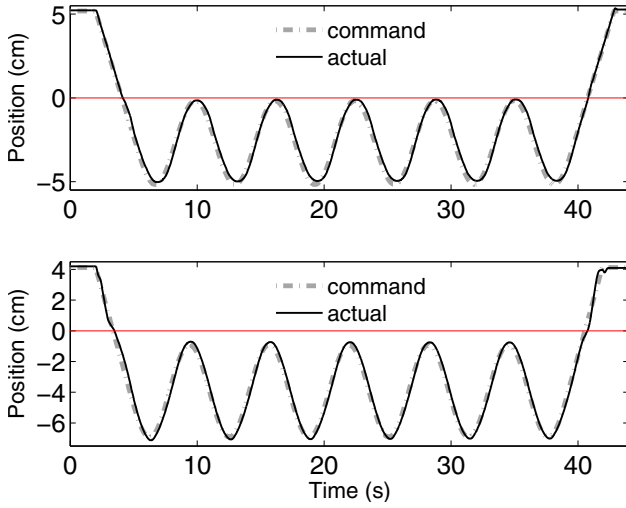


Fig. 2. Examples of reference trajectories for the end-effector position (dashed lines) used in the identification experiments for the sponge (top) and the dice (bottom). Actual movements of the end-effector are also shown by solid lines.

generating high forces and hitting saturation limits of the joint torques.

This experiment is performed 10 times for each surface. During the experiments, we recorded the position and velocity of the end-effector (\mathbf{r} and $\dot{\mathbf{r}}$) and the contact forces (\mathbf{f}_s) at every 10ms. Then, by using (8), (9) and (10), we computed the contact normal force (f), the surface deformation (z) and its rate (\dot{z}) and put them in column vectors $\boldsymbol{\sigma}$, $\boldsymbol{\zeta}$ and $\boldsymbol{\nu}$, respectively. So,

$$\boldsymbol{\sigma} = \begin{bmatrix} f_{t_1} \\ f_{t_2} \\ \vdots \\ f_{t_n} \end{bmatrix}, \quad \boldsymbol{\zeta} = \begin{bmatrix} z_{t_1} \\ z_{t_2} \\ \vdots \\ z_{t_n} \end{bmatrix}, \quad \boldsymbol{\nu} = \begin{bmatrix} \dot{z}_{t_1} \\ \dot{z}_{t_2} \\ \vdots \\ \dot{z}_{t_n} \end{bmatrix},$$

where t_1, t_2, \dots, t_n are the time instants. Using the collected data, we estimated the parameters k and λ for the three contact models as follows. For the Kelvin-Voigt linear model, the relationship between the normal forces and the deformations can be described as $\boldsymbol{\sigma} = \mathbf{A}[k \ \lambda]^T$, where $\mathbf{A} = [\boldsymbol{\zeta} \ \boldsymbol{\nu}]$. By employing linear least-squared regression [14], the unique solution for k and λ will be

$$[\hat{k} \ \hat{\lambda}]^T = (\mathbf{A}^T \mathbf{A})^{-1} \mathbf{A}^T \boldsymbol{\sigma}, \quad (16)$$

where \hat{k} and $\hat{\lambda}$ are the estimated parameters of the contact models. To estimate the parameters of the non-linear models, we redefine \mathbf{A} as $[\boldsymbol{\zeta}^{\frac{3}{2}} \ \boldsymbol{\zeta}^{\frac{3}{2}} \boldsymbol{\nu}]$ for the Hunt-Crossley and $[\boldsymbol{\zeta}^{\frac{3}{2}} \ \boldsymbol{\zeta}^{\frac{1}{2}} \boldsymbol{\nu}]$ for the Azad-Featherstone model. After estimating the parameters, the estimated normal force ($\hat{\sigma}$) can be calculated as

$$\hat{\sigma} = \mathbf{A}[\hat{k} \ \hat{\lambda}]^T. \quad (17)$$

To select the best model for each surface, we compare the three contact models in fitting the actual data. Our comparison criterion is based on the *fitness value*, which is

TABLE I

FITNESS VALUES OF THREE DIFFERENT CONTACT MODELS FOR EACH SURFACE CALCULATED VIA (18)

	linear K/V	non-linear H/C	non-linear A/F
sponge	0.965 ± 0.001	0.981 ± 0.001	0.986 ± 0.001
dice	0.976 ± 0.001	0.845 ± 0.002	0.853 ± 0.002

TABLE II

ABSOLUTE VALUES OF THE ERRORS BETWEEN THE COMMAND AND ACTUAL FORCES FOR THE SPONGE SURFACE. FORCES ARE IN NEWTONS.

ratios	0.8	0.4	0.7	0.3	0.5	0.6
commands	224	112	196	84	140	168
cycle #1	30.49	14.33	15.25	13.56	17.46	15.93
cycle #2	15.45	4.92	9.47	7.43	12.45	13.16
cycle #3	16.02	5.38	11.69	6.33	11.56	13.70
cycle #4	18.01	5.10	12.59	5.47	10.72	13.69
ratios	0.75	0.35	0.65	0.25	0.45	0.55
commands	210	98	182	70	126	154
cycle #5	17.23	5.30	14.06	6.23	12.80	13.09

calculated via

$$\text{fitness} = 1 - \left(\frac{\sum (\boldsymbol{\sigma} - \hat{\boldsymbol{\sigma}})^2}{\sum (\boldsymbol{\sigma} - \bar{\boldsymbol{\sigma}})^2} \right), \quad (18)$$

where $\bar{\boldsymbol{\sigma}}$ is the average value of $\boldsymbol{\sigma}$. For an unbiased assessment, we employed a 5-fold cross validation technique [12]. The average and standard deviation of fitness values for each surface are shown in Table I. As can be seen in this table, although the two non-linear models have almost the same fitness for each surface, the Azad-Featherstone model is better than the Hunt-Crossley one in both cases. These two are better than the linear model for the sponge surface whereas the linear model provides a better fit for the dice surface. Therefore, to control the contact forces in the next experiments (subsection III-C), we use the Azad-Featherstone model for the sponge and the linear model for the dice surface.

C. Control Experiments

To verify the proposed method in Section II for controlling the normal contact force, we study the performance of the controller in reaching various command forces. A set of 30 command forces are defined for each surface. Each set consists of 12 different values which 6 of them are repeated 4 times and then followed by the other 6 values; 30 in total. These 12 command forces are computed for each surface based on the maximum recorded normal force during the identification experiments. The maximum forces were 280N and 130N for the sponge and dice surfaces, respectively. The values of the command forces and also the ratio between each command force and the maximum force are mentioned in Tables II and III for the sponge and dice, respectively.

By using the corresponding contact model for each surface, we convert force commands to deformation commands which are actually position commands for the end-effector in the vertical direction (by using (9)). This conversion can be done by using (2) as

$$z^{cmd} = \left(\frac{f^{cmd}}{\hat{k}} \right)^{\frac{1}{a}}, \quad (19)$$

TABLE III

ABSOLUTE VALUES OF THE ERRORS BETWEEN THE COMMAND AND ACTUAL FORCES FOR THE DICE SURFACE. FORCES ARE IN NEWTONS.

ratios	0.8	0.4	0.7	0.3	0.5	0.6
commands	104	52	91	39	65	78
cycle #1	15.81	8.02	8.73	9.62	9.67	7.42
cycle #2	2.26	1.51	2.89	5.61	5.39	3.57
cycle #3	7.13	0.95	3.49	4.04	4.72	3.85
cycle #4	8.30	0.10	3.94	3.38	4.51	3.43
ratios	0.75	0.35	0.65	0.25	0.45	0.55
commands	97.5	45.5	84.5	32.5	58.5	71.5
cycle #5	6.65	1.58	4.56	5.30	5.97	4.59

where $a = 1$ for the dice (linear model) and $a = \frac{3}{2}$ for the sponge (non-linear model) surfaces. Note that, we expect zero velocity of the end-effector at the time of reaching force commands (i.e. setting $\dot{z} = 0$ in (2)). To command the end-effector of the robot, to move from one position command to the next one, we define a time dependent reference trajectory for its position. In order to make sure that the results are not dependent on a certain trajectory type, we do not use a sine function as we did for the identification experiments. Instead, we use a fifth-order polynomial function as a reference trajectory for the end-effector's position. The time length of the trajectory is set to 2 seconds. Therefore, to achieve all force commands, the whole reference trajectory of the end-effector is formed of 30 fifth-order polynomial trajectories which connect the position commands to each other (60s in total). The reference velocity and acceleration (\dot{z}^{cmd} and \ddot{z}^{cmd} to be used in (11)) are calculated by differentiating the fifth-order reference trajectory of the position.

Figs. 3 and 4 show the actual force profiles together with the predicted ones and also the command forces for the sponge and dice surfaces, respectively. The predicted force profiles are calculated by feeding the command values of the deformations and their rates (z^{cmd} and \dot{z}^{cmd}) into corresponding contact models. The command forces are shown by green circles in the plots. Each graph is divided by red dashed lines into 5 regions representing 5 cycles of commands: the first 6 commands are repeated 4 times and then followed by 6 different commands in the fifth cycle. The duration of each cycle is 12s since it is formed of 6 points which are placed 2 seconds apart. The values of the command forces and also absolute errors of reaching those values are mentioned in Tables II and III for both surfaces.

In the first cycle of commands, to convert the force commands to deformation commands via (19), we used \hat{k} that was already estimated for each surface during the identification experiments. Also, to calculate the predicted force profiles in Figs. 3 and 4 for the first cycle, \hat{k} and $\hat{\lambda}$ are those obtained from identification experiments. According to Tables II and III, the errors are between %7 to %16 for the sponge and %7 to %25 for the dice in the first cycle.

From the end of the first cycle till the end of the experiment for each surface, we update the contact parameters in order to decrease the errors between actual and command forces. To update the parameters via (16), we use the

recorded data during the last 12s (i.e. 1200 points since the sample rate is 10ms). This strategy allows us to improve the estimation of the model parameters without substantially affecting the computation time.

The effects of this update can be seen by comparing the errors of the first cycle with the ones for the second, third and fourth cycles in Tables II and III. According to these tables, the maximum errors in the first four cycles are %16, %9, %8 and %8 for the sponge and %25, %14, %10 and %9 for the dice, respectively. Regarding these numbers, it is obvious that updating the contact parameters significantly improved the accuracy of reaching the command forces. This improvement is also visible in Figs. 3 and 4. It can be seen in these figures that the predicted force profile starts to fit the actual one better just after the end of the first cycle.

In the last cycle, we show the performance of our online updating strategy in realizing new force commands. As already mentioned, the force commands in the last cycle are different from the previous ones. These forces and also their corresponding errors are mentioned in the lower parts of Tables II and III. The maximum errors of the last cycle are %10 and %16 for the sponge and dice, respectively. Comparing these numbers with the maximum errors of the other cycles which are mentioned above, suggests that although the errors are increased in the last cycle they are still much lower than the first cycle. It implies that introducing new command forces does not affect the performance of the controller while the contact parameters are updated online.

IV. CONCLUSION AND FUTURE WORK

In this paper, we converted the problem of controlling compliant contact normal forces to controlling surface deformations by using contact models. We explained how this can be included inside a whole-body motion control framework for a humanoid robot. To study the performance of the proposed method in practice, a series of experiments, including identification and control experiments, were performed with a LWR KUKA manipulator. During the identification experiments, we estimated the contact models between the robot's end-effector and two soft surfaces using least-squared linear regression algorithm. In control experiments, by using the estimated models, we controlled the robot's motion in order to achieve various desired contact normal forces for each surface. We also studied the effects of updating model parameters during control experiments using an online estimation method. The experiment results showed that desired forces can be achieved with some errors while using the estimated model from identification experiments. These errors are decreased substantially by online adaptation of the contact model parameters during control experiments. For the future work, we are planning to extend the current work to control the CoP of the contact as well.

ACKNOWLEDGMENT

The work presented in this paper is supported by the European Community Framework Programme 7 through the CoDyCo project, contract no. 600716.

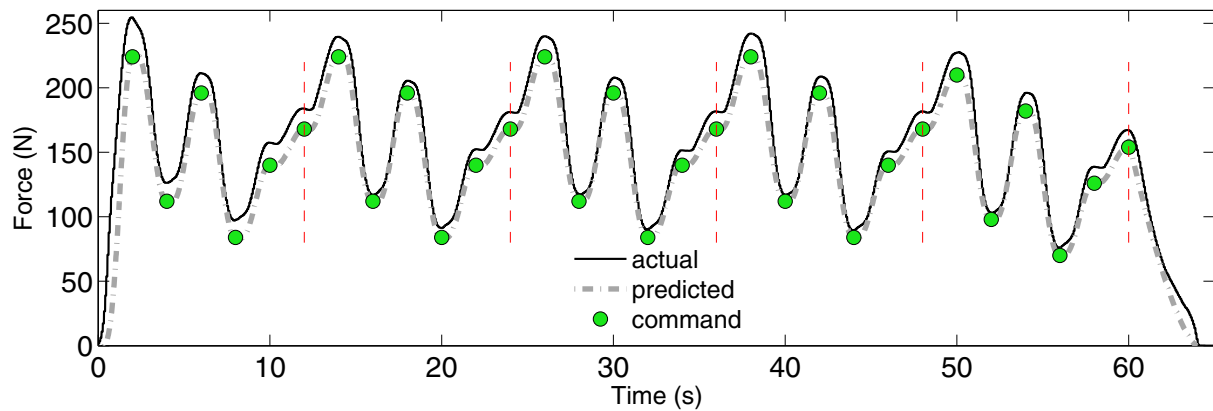


Fig. 3. Actual, predicted and command normal contact forces for the sponge surface.

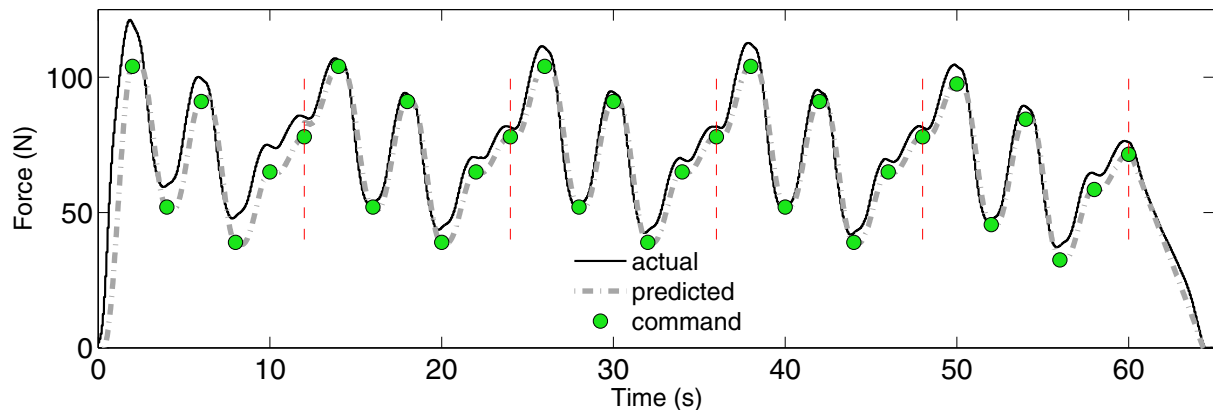


Fig. 4. Actual, predicted and command normal contact forces for the dice surface.

REFERENCES

- [1] M. Azad and R. Featherstone. Modelling the contact between a rolling sphere and a compliant ground plane. *Australasian Conf. Robotics and Automation*, Brisbane, Australia, 1–3 Dec 2010.
- [2] M. Azad and R. Featherstone. A new nonlinear model of contact normal force. *IEEE Trans. Robotics*, 30(3):736–739, June 2014.
- [3] M. Azad and M. Mistry. Balance control strategy for legged robots with compliant contacts. *Proc. IEEE Int. Conf. Robotics and Automation*, pp. 4391–4396, Seattle, WA, 26–30 May 2015.
- [4] K. Bouyarmane and A. Kheddar. FEM-based static posture planning for a humanoid on deformable contact support. *Proc. IEEE-RAS Int. Conf. Humanoid Robots*, pp. 487–492, Bled, Slovenia, 26–28 Oct 2011.
- [5] N. Diolaiti, C. Melchiorri and S. Stramigioli. Contact impedance estimation for robotic systems. *IEEE Trans. Robotics*, 21(5):925–935, Oct 2005.
- [6] W. Fluggè. *Viscoelasticity*. Waltham, Mass.:Blaisdell Publishing Company 1967.
- [7] G. Gilardi and I. Sharf. Literature survey of contact dynamics modelling. *Mechanism and Machine Theory*, 37(10):1213–1239, Oct 2002.
- [8] A. Haddadi and K. Hashtrudi-Zaad. A new method for online parameter estimation of Hunt-Crossley environment dynamic models. *Proc. IEEE/RSJ Int. Conf. Intelligent Robots and Systems*, pp. 981–986, Nice, France, 22–26 Sep 2008.
- [9] A. Haddadi and K. Hashtrudi-Zaad. Real-time identification of Hunt-Crossley dynamic models of contact environment. *IEEE Trans. Robotics*, 28(3):555–566, June 2012.
- [10] B. Henze, M. Roa and C. Ott. Passivity-based whole-body balancing for torque-controlled humanoid robots in multi-contact scenarios. *Int. Journal of Robotics Research*, 2016.
- [11] K. Hunt and F. Crossley. Coefficient of restitution interpreted as damping in vibroimpact. *Journal of Applied Mechanics*, 42(2):440–445, June 1975.
- [12] R. Kohavi. A study of cross-validation and bootstrap for accuracy estimation and model selection. *Proc. Int. Joint Conf. Artificial Intelligence*, 14:1137–1145, 1995.
- [13] S. H. Lee and A. Goswami. A momentum-based balance controller for humanoid robots on non-level and non-stationary ground. *Autonomous Robots*, 33(4):399–414, Apr 2012.
- [14] D. Luenberger. *Optimization by vector space methods*. John Wiley & Sons, 1969.
- [15] L. Righetti, J. Buchli, M. Mistry and S. Schaal. Inverse dynamics control of floating-base robots with external constraints: a unified view. *Proc. IEEE Int. Conf. Robotics and Automation*, pp. 1085–1090, Shanghai, China, 9–13 May, 2011.
- [16] L. Righetti and S. Schaal. Quadratic programming for inverse dynamics with optimal distribution of contact forces. *Proc. IEEE-RAS Int. Conf. Humanoid Robots*, pp. 538–543, Osaka, Japan, 29 Nov–1 Dec, 2012.
- [17] L. Saab, O. Ramos, N. Mansard, P. Soueres and J. Fourquet. Generic dynamic motion generation with multiple unilateral constraints. *Proc. IEEE/RSJ Int. Conf. Intelligent Robots and Systems*, pp. 4127–4133, San Francisco, CA, 25–30 Sep 2011.
- [18] J. Salini, V. Padois and P. Bidaud. Synthesis of complex humanoid whole-body behavior: A focus on sequencing and task transitions. *Proc. IEEE Int. Conf. Robotics and Automation*, pp. 1283–1290, Shanghai, China, 9–13 May 2011.
- [19] R. Schindeler and K. Hashtrudi-Zaad. Polynomial linearization for real-time identification of environment Hunt-Crossley models. *Haptics Symposium*, pp. 173–178, Philadelphia, Pennsylvania, 8–11 Apr 2016.
- [20] B. Stephens and C. Atkeson. Dynamic balance force control for compliant humanoid robots. *Proc. IEEE/RSJ Int. Conf. Intelligent Robots and Systems*, pp. 1248–1255, Taipei, Taiwan, 18–22 Oct 2010.
- [21] N. Xydes and I. Kao. Modeling of contact mechanics and friction limit surfaces for soft fingers in robotics with experimental results. *Int. Journal of Robotics Research*, 18(9):941–950, Sep 1999.